Available online at www.sciencedirect.com
SCIENCE DIRECT
International Journal of Heat and Fluid Flow 26 (2005) 894–904
International Journal of HEAT AND FLUID FLOW
www.elsevier.com/locate/ijhff

Vortex shedding induced by a solitary wave propagating over a submerged vertical plate

Chang Lin [a,*], Tsung-Chun Ho [a], Sung-Chieh Chang [a], Shih-Chun Hsieh [a], Kuang-An Chang [b]

[a] Department of Civil Engineering, National Chung Hsing University, Taichung 402, Taiwan
[b] Department of Civil Engineering, Texas A&M University, College Station, TX 77843-3136, USA

Available online 9 November 2005

Abstract

Experimental study was conducted on the vortex shedding process induced by the interaction between a solitary wave and a submerged vertical plate. Particle image velocimetry (PIV) was used for quantitative velocity measurement while a particle tracing technique was used for qualitative flow visualization. Vortices are generated at the tip of each side of the plate. The largest vortices at each side of the plate eventually grow to the size of the water depth. Although the fluid motion under the solitary wave is only translatory, vortices are shed in both the upstream and downstream directions due to the interaction of the generated vortices as well as the vortices with the plate and the bottom. The process can be divided into four phases: the formation of a separated shear layer, the generation and shedding of vortices, the formation of a vertical jet, and the impingement of the jet onto the free surface. Similarity velocity profiles were found both in the separated shear layer and in the vertical jet.

Keywords: Wave–structure interaction; Solitary waves; Flow visualization; Particle image velocimetry

1. Introduction

A submerged structure in a coastal zone, such as a breakwater or an artificial reef, has been employed in many engineering practices to dissipate wave energy, reduce beach erosion, and for sustainable development. As waves propagate over the structure, part of the wave energy is reflected back to the open ocean, part of the energy is transmitted to the beach, and part of the energy is converted to turbulence and dissipated in the vicinity of the structures. Potential flow has been a good assumption in formulating the problem before waves encounter the structure. After the encounter, the potential flow assumption may still be reasonable for estimating the reflected and transmitted wave height, but it is no longer applicable in predicting the velocity field in the vicinity of the structure due to the vortical and turbulent nature of the flow. Flow separation at the structure induces and sheds vortices both offshore and onshore in a limited region around the structure. While the induced vortices help to dissipate the wave energy, the generated strong vortices may hamper the structure integrity and stability due to scour. On the other hand, the vortices increase the exchange between the bottom water and surface water, and sustain the health of the coastal ecology and environment similar to the upwelling effect in a lake.

A structure with a simplified geometry such as a rectangle has been used in most theoretical, numerical, and experimental studies for the understanding of the interaction between structures and waves. Among many others, Mei and Black (1969), Tang and Chang (1998), Ting and Kim (1994), Zhuang and Lee (1996), Huang and Dong (1999, 2001), Chang et al. (2001, 2005), Lin (2004), Sue et al. (2005), and Lin et al. (in press-a) have all used a rectangular dike in their study of the problem. Typically the length of the structure is in the same order or greater than the

* Corresponding author. Tel./fax: +886 4 2285 5182.
E-mail address: clin@mail.ce.nchu.edu.tw (C. Lin).

0142-727X/$ - see front matter © 2005 Published by Elsevier Inc.
doi:10.1016/j.ijheatfluidflow.2005.10.009

height of the structure. For a limited cases and applications, the length of the structure is much smaller than its height, and typically represented by a vertical plate (Ono et al., 1997; Sue et al., 2005). Moreover, solitary waves have been frequently used in the study due to their simple and permanent wave form and, in some applications, representation of a tsunami due to its shallow water nature. While most existing investigations focused on the prediction of wave energy transmission and reflection and wave transformation (e.g., Mei and Black, 1969; Lin, 2004), more and more recent studies have started to investigate the turbulent and vortical structure of the flow to gain more insight on the generation and evolution of the vortices induced at the corners of the submerged structure.

Numerical models based on Navier–Stokes equations and their derivatives to account for the viscous and rotational effects in the flow have been used to compute the interaction between waves and structures in the recent decade. More realistic flow fields were obtained by examining the calculated results, although most results were either validated qualitatively or not validated at all due to the lack of detailed experimental measurements (Tang and Chang, 1998; Huang and Dong, 1999, 2001; Lin, 2004; Sue et al., 2005). Only very few computations were validated quantitatively with detailed velocity comparisons at several cross sections and time steps (Chang et al., 2001), and some have been validated with velocity measurements at a small number of points (Zhuang and Lee, 1996). The reason may be partially contributed from the difficulty of accurately modeling the vortex generation mechanism due to flow separation, which requires an extremely fine resolution or a precise formulation of the boundary layer near the structure corners, and partially contributed from the difficulty of obtaining quantitative experimental data, including velocity and turbulence, covering the vicinity of the structure.

Experimental measurements applying more advanced optics and imaging techniques such as laser Doppler velocimetry (LDV) and particle image velocimetry (PIV) have been started and employed in the study to obtain both time history velocity data at a point and flow maps at a give plane since last decade. Quantitative velocity information was obtained for the study of a solitary wave interaction with a rectangular dike (Zhuang and Lee, 1996; Chang et al., 2001; Lin et al., in press-a). In addition, researchers also applied qualitative flow visualization techniques to take advantage of their higher spatial resolution in comparison to the quantitative velocity measurement, and better identification of the vortex structure. However, detailed measurements on the case of a solitary wave propagating over a thin plate have rarely been studied using the advanced measurement techniques, even though the study is important in the understanding of the coastal environment.

The objective of this study is to elucidate the temporal and spatial dependence of vortex structure induced by a solitary wave propagating over a submerged vertical plate experimentally. The PIV and particle tracing techniques were used for velocity measurements and flow visualization. Flow similarities were examined by relating the measured velocity field to a shear layer and a turbulent jet.

2. Experimental setup

The experiments were conducted in a glass-walled and glass-bottomed wave flume at the Department of Civil Engineering, National Chung Hsing University. The flume is 8.85 m long, 0.50 m wide, and 0.50 m deep and used for both the wave and current studies. A piston-type wavemaker driven by a variable-speed motor was installed at one end of the flume. The wavemaker was originally designed to generate monochromatic waves. An electromagnetic clutch was installed inside the wavemaker to allow a rapid start and stop of the wave paddle for the generation of the desired solitary waves. The generated solitary waves are followed by a dispersive tail wave train that has an amplitude one order of magnitude smaller than that of the solitary waves. Although the generation mechanism is not ideal, the generated solitary waves were clean enough for the present study with certain combinations of wave height and water depth. The generated solitary waves were also found to be highly repeatable. Two capacitance-type wave gauges separated at a distance of 6.0 cm in the streamwise direction were used to measure the free surface elevations. The wave celerity was obtained through cross correlating these two measured free surface profiles.

The target solitary wave used throughout the present study has a wave height of $H = 1.2$ cm in a water depth of $h = 7.0$ cm. The use of the specific wave parameters was because the combination gives the best waveform without losing its generality in the study. Before the installation of the structure in the flume, validation on the generated wave was performed by comparing the free surface displacement and the wave celerity. Fig. 1(a) shows the comparison of the free surface profile between the generated solitary wave and the theoretical wave form of

$$\eta(x,t) = H\operatorname{sech}^2\left[\sqrt{\frac{3H}{4h^3}}(x-ct)\right] \tag{1}$$

where η denotes the free surface elevation above the still water level, x and t the streamwise direction and time, and c the wave celerity that can be calculated theoretically as $c = \sqrt{g(h+H)}$. Very good agreement between the generated wave and the theory was obtained. Fig. 1(b) shows the comparison of the wave celerity. The generated waves agree very well with the data reported in Daily and Stephan (1953), and both show a slightly lower celerity than the theoretical value. Comparisons on the fluid particle velocity under the wave crest were also performed and reported in Lin et al., in press-a). To illustrate the inflow condition, Fig. 1(c) shows the velocity field under the solitary waves. In this figure, the vertical coordinate Y represents the height above the bottom of the wave flume. Note that

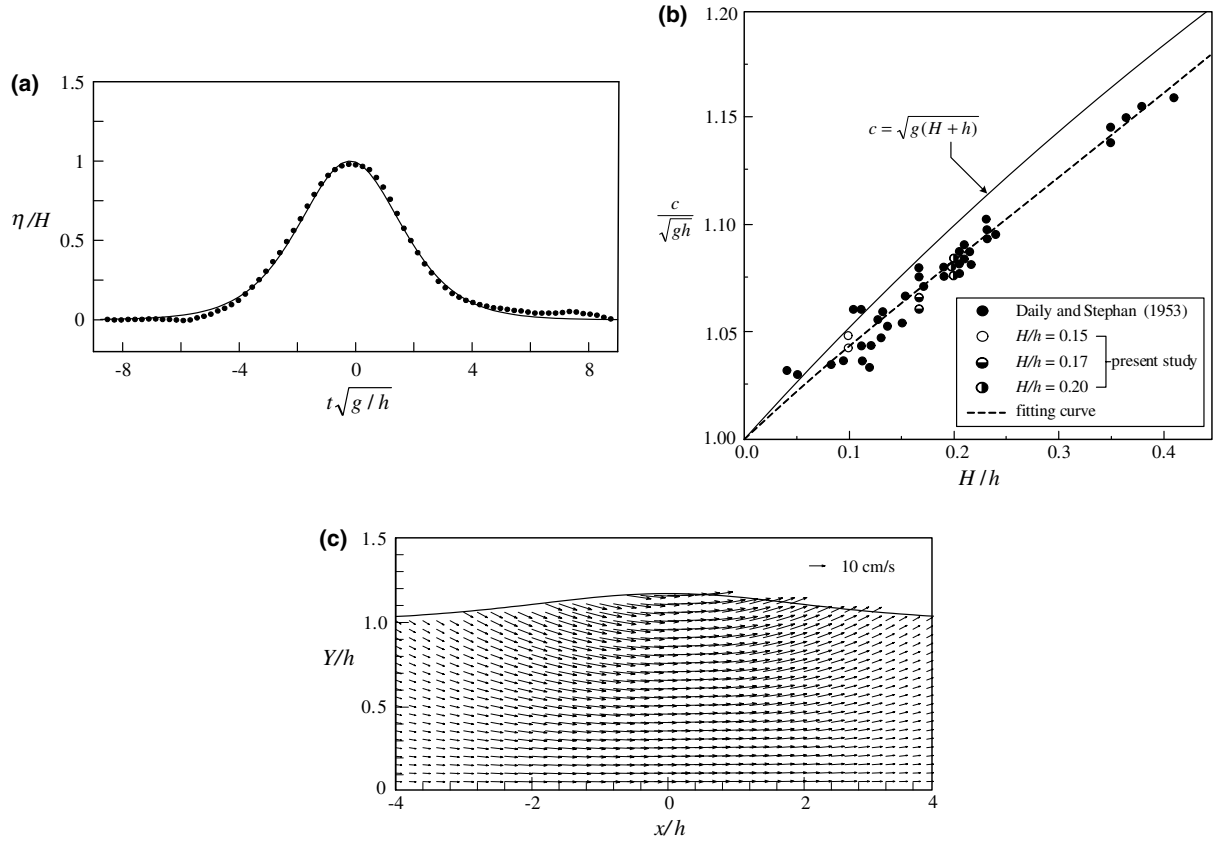

Fig. 1. Validation of target solitary wave with $H = 1.2$ cm and $h = 7.0$ cm. (a) Comparison of free surface profile: (●) wave gauge measurement; (—) theory. (b) Comparison of wave celerity. (c) Velocity field under the solitary wave obtained using PIV.

the solitary wavelength is much greater than the water depth and the field of view of particle image velocimetry (PIV) so the velocity presented here is composed from the PIV measurements at several different time steps. Details on the PIV system will be described later.

A schematic diagram of the wave flume with the submerged vertical plate mounted on the bottom is shown in Fig. 2. The plate was made of acrylic and located near the middle the flume. The plate has a spanwise width the same as that of the flume, a vertical height of $D = 3.0$ cm, and a thickness of $L = 0.43$ cm. To eliminate

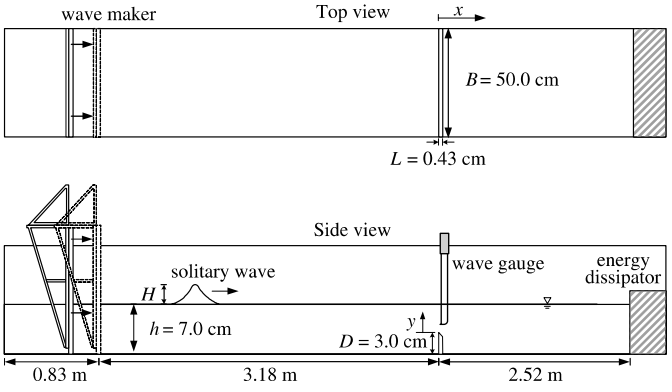

Fig. 2. Sketch of the wave flume and the vertical plate.

the after-body effect, the top of the plate was sharpened at an angle of 45°. The still water depth, h, was kept constant as 7.0 cm throughout the experiments while the target solitary wave height was kept as $H = 1.2$ cm. This gives $H/h = 0.17$, $D/h = 0.43$, and $L/D = 0.14$ in the present study. The coordinate system is also shown in Fig. 2 and defined as follow: The origin $(x, y) = (0, 0)$ is at the upstream side of the plate and the tip of the plate, respectively. In addition, $t = 0$ is defined at the moment when the crest of the solitary wave is at $x = 0$. The Reynolds number is about 19,000 in the present study. The Reynolds number is defined following Chang et al. (2005), i.e., $Re = Uh/v$ in which the characteristic velocity U is defined as $U = u_m h/(h - D)$ with $u_m (= \frac{H}{h}\sqrt{g(h+H)})$ being the maximum particle velocity of the solitary wave to account for the existence of the submerged structure.

Aluminum powder or titanium dioxide powder were uniformly introduced into the water as the tracing particles for qualitative flow visualization in the particle tracing technique. The particles form pathlines if illuminated by a laser light sheet and captured using a camera with the exposure time appropriately adjusted. A 5 W argon-ion laser (Coherent 90 series) was diverged through a cylindrical lens to form the light sheet of about 1.5 mm in thickness. The light sheet entered the wave flume vertically through the glass bottom along the flume centerline at

the location of the plate to illuminate the tracing particles on a two-dimensional vertical plane. High resolution cameras, including a Nikon F5 film cameras and a Nikon D100 digital camera, were employed to take images, and a digital video camera (Sony DCR-TRV70) was used to record the temporal variation of vortex shedding processes in the vicinity of the plate.

A PIV system was used to measure the two-dimensional velocity field on the same vertical light sheet plane as that in the particle tracing technique. The light source is a dual-head frequency-doubled Nd:YAG laser (Continuum Surelite). The maximum energy output is 200 mJ per pulse in 532 nm wavelength. The pulse duration is 10 ns and the repetition rate is 15 Hz for each laser head. The image recording system is an 8-bit digital CCD camera (TSI Pivcam 10–30) which has a 1016×1000 pixels resolution and a maximum framing rate of 30 frames/s. Cross-correlation analysis using commercial software (TSI Insight) was performed to obtain the two-dimensional velocity fields. Interrogation windows of 32×32 pixels with a 50% overlap were used in the velocity determination.

3. Results and discussion

Images taken using the particle tracing technique are demonstrated in Fig. 3. Although qualitative, the fine resolution images do provide a clear picture on the generation and evolution of the vortices through the pathlines as well as the profile of the free surface. Note that $t = 0$ is defined as the instant when the crest of the solitary wave is at the top of the plate. Fig. 3(a)–(c) show the generation of a clockwise vortex at the tip of the plate due to the approaching wave that causes the flow to separate at the tip. The main vortex generated in Fig. 3(a)–(c) eventually sheds out and continues to grow in size, as shown in Fig. 3(d)–(f). Note that there is a second clockwise vortex generated at the tip of the plate in Fig. 3(c). The size of this tiny vortex is approximately the thickness of the plate. It may be caused by the thin yet finite width of the plate, similar to that observed in waves interacting with a dike (Lin et al., in press-a). After the size of the main vortex growing to almost the depth of the water in Fig. 3(f), the translatory motion of fluid particles has almost completely ceased as the wave past. This large vortex is confined by the bottom of the tank and the rear edge of the plate. It forces the water to move upward at the rear edge of the plate. This creates a counterclockwise vortex above the tip of the plate and causes the previously generated tiny near-tip vortex to disappear because of the interaction of vortices of different signs. The counterclockwise vortex continues to move upward and upstream and grow larger. Subsequently, the main clockwise and counterclockwise vortices reach the free surface and cause the free surface to bulge, as shown in Fig. 3(g) and (h). A second counterclockwise vortex is generated near the junction between the bottom and the plate at the trailing side. A third counterclockwise vortex also appears near the surface at $x/h \approx 1$ (or $x \approx 7.0$ cm) induced by the interaction between the main clockwise vortex and the free surface.

The flow pattern shown in Fig. 3 is further supported by the PIV measurements in Fig. 4. Fig. 4(a)–(d) show the formation of the main clockwise vortex starting before the arrival of the wave crest to the passage of the crest. The tiny vortex at the tip of the plate shown in Fig. 3(c) is not captured in the velocity map due to the much coarser resolution in the PIV measurements. This marks the need of the extra flow visualization in addition to the PIV measurements. By carefully examining the flow field, the flow pattern shows certain similarity with that of a shear layer at $x/h > 0$ before the passage of the wave crest, especially during $-12.0 \leqslant t\sqrt{g/h} \leqslant -6.0$, and can be seen in Fig. 4(a). The vortex starts to form and sheds out after this stage, as shown in Fig. 4(a)–(e). Subsequently, a strong vertical velocity similar to a jet at the edge of the plate at $x/h \approx 0$ is observed during the period of $10.0 \leqslant t\sqrt{g/h} \leqslant 24.0$, which is shown in Fig. 4(f) and (g). A similar jet-like pattern near the submerged structure was also observed in Zhuang and Lee (1996) and Lin et al. (in press-a), although in their studies a dike with a dimension of $L/D = \mathrm{O}(1\text{–}10)$ was used. After this stage the vertical jet impinges the free surface while the counter rotating vortex pair continues to move upward, encounters the free surface, bounces downward, and distances from each other, as shown in Fig. 4(f)–(h). The flow pattern is somewhat similar to an impinging jet even though the vortices at each side of the jet axis are asymmetric. The vortex pair eventually diffuses and grows to the size of the water depth (not shown here).

Based on the observation made from Figs. 3 and 4, we categorize the interaction process into four phases: formation of a separated shear layer, generation and shedding of vortices, formation of a vertical jet, and impingement of the jet onto the free surface. We further examine the PIV measurements to check whether any similarities exist.

3.1. Formation of a separated shear layer

Detailed velocity information is extracted from the PIV velocity maps. Note that the propagation of the solitary wave over the vertical plate is unsteady so the velocity distribution along a given cross section is a function of time. Fig. 5 shows the variation of the horizontal velocity distributions at six different vertical cross sections between $x/h = 0.0$ and $x/h = 0.121$ (downstream from the front edge of the vertical plate) during the period of $-12.0 \leqslant t\sqrt{g/h} \leqslant -6.0$. The period corresponds to the formation of a separated shear layer downstream of the vertical plate. It is found that the velocity at each cross section becomes relatively uniform at $y > 1.5$ cm and $y < -1.0$ cm. The figure shows the unsteady nature of the problem. Interestingly, velocity overshooting due to flow separation is observed in each velocity profile between $y = -1.0$ cm and $y = 1.5$ cm. It should be pointed out that velocity overshooting was also observed in other separated flows.

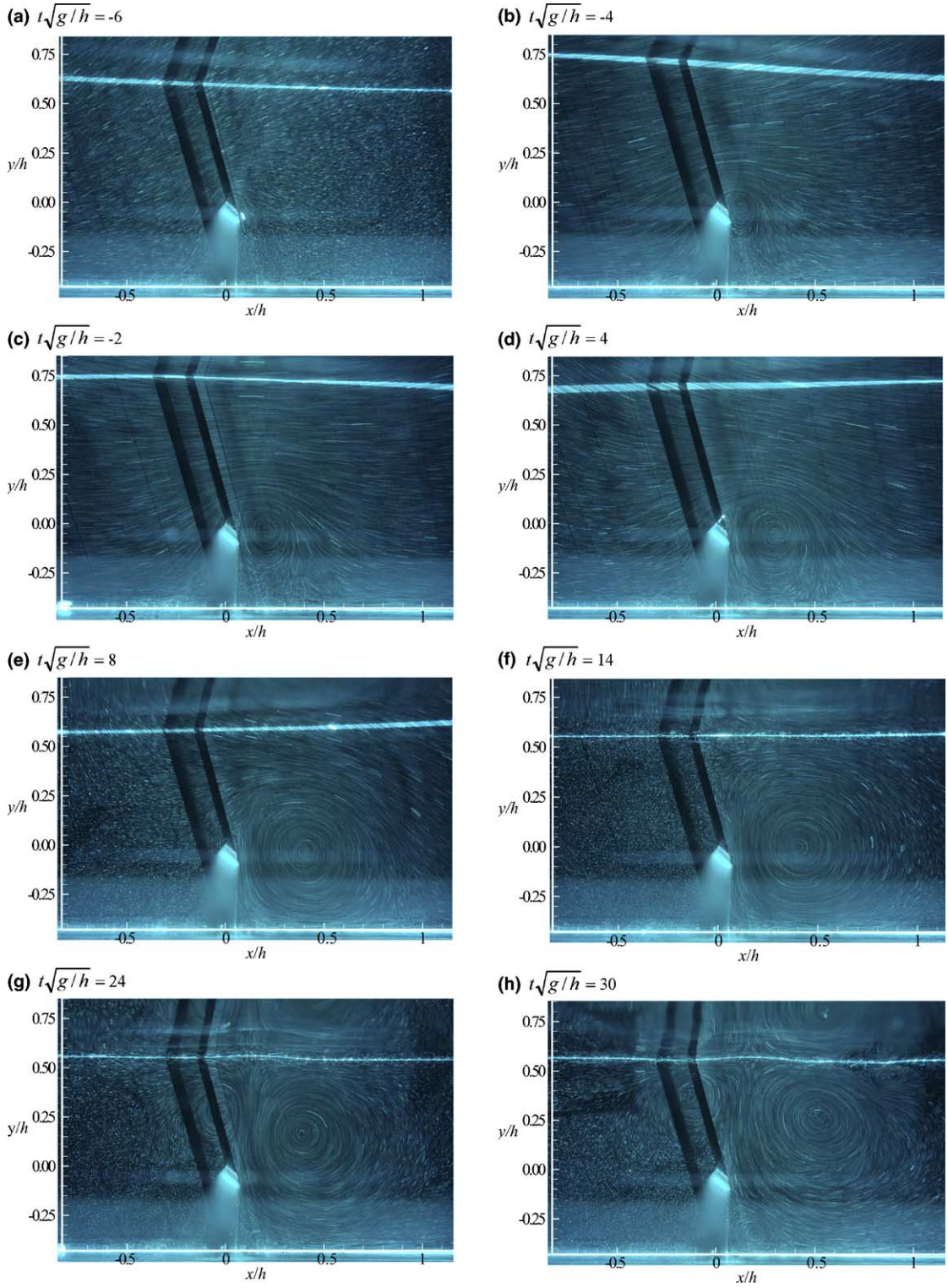

Fig. 3. Images taken using the particle tracing technique at $t\sqrt{g/h}$ = (a) −6.0, (b) −4.0, (c) −2.0, (d) 4.0, (e) 8.0, (f) 14.0, (g) 24.0, and (h) 30.0.

Examples are the flows at the lee side of a two-dimensional solid fence (e.g., Gupta and Ranga-Raju, 1987), and in the near-wake flow of a two-dimensional circular cylinder (e.g., Kravchenko and Moin, 2000; Lin et al., 2004), although these studies are under the steady free-stream velocity condition. After trying several length scales and velocity scales, Fig. 6 shows the schematic profile of the separated shear layer with the final length and velocity scales. In the figure, u_{max} denotes the maximum horizontal velocity (i.e., the maximum overshooting velocity), y_{max} the value of y where u_{max} occurs, u_{min} the uniform velocity at $y < -1.0$ cm, b_1 the length scale representing the value of y at $u = u_{max}/2$

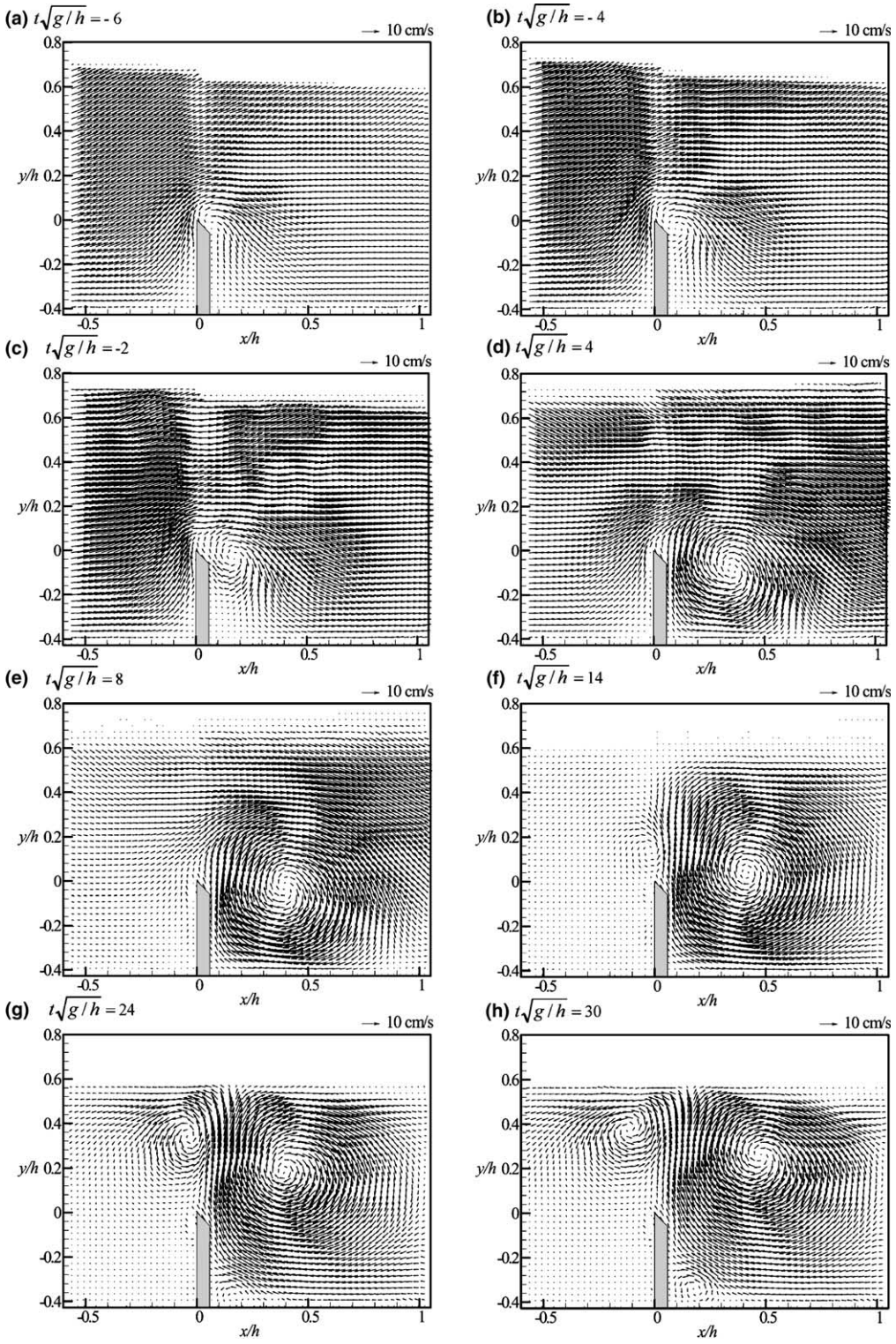

Fig. 4. PIV velocity maps measured at $t\sqrt{g/h}$ = (a) −6.0, (b) −4.0, (c) −2.0, (d) 4.0, (e) 8.0, (f) 14.0, (g) 24.0, and (h) 30.0.

(i.e., the half-width of the shear layer). Note that all these velocity and length scales are not constant but time dependent due to the unsteady inflow condition of the solitary wave.

In order to estimate more accurately the values of u_{max}, u_{min}, y_{max}, and b_1 during $-12.0 \leqslant t\sqrt{g/h} \leqslant -6.0$, nonlinear curve fittings to the experimental data were performed (to the data points in Fig. 5). Fig. 7(a) and (b) illustrate the trends of the two velocity scales, u_{max} and u_{min}, against time, t, for $0 < x/h \leqslant 0.121$. One can see that both u_{max} and u_{min} increase linearly with the increase of t except that u_{min} is equal to zero between $x/h = 0$ and $x/h = 0.039$. In addition,

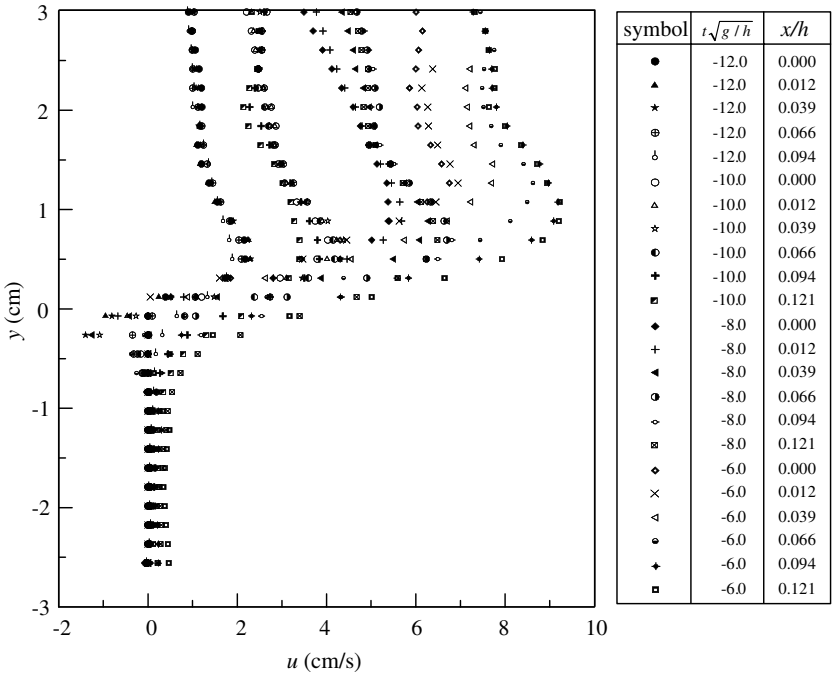

Fig. 5. Variation of the horizontal velocity distributions measured at six different vertical cross sections between $x/h = 0.0$ and 0.121.

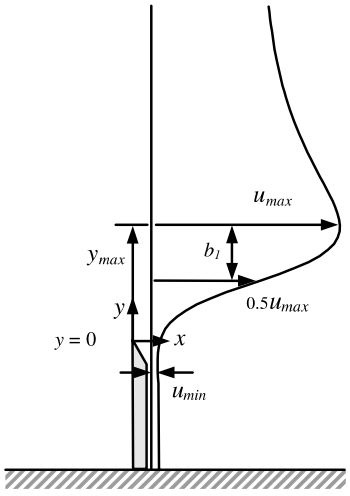

Fig. 6. Schematic sketch of the separated shear layer.

the variations of the two length scales, $y_{\max}$ and b_1, with respect to t are presented in Fig. 7(c) and (d). It is found that both $y_{\max}$ and b_1 increase as t increases, though the relationship is no longer linear. Based on the observation above, we expect that $(u_{\max} - u_{\min})$ and b_1 could be the characteristic scales, while $u_{\min}$ and $y_{\max}$ could be considered as the references (or the shifting factors). Accordingly, the dimensionless horizontal velocity deficit $(u - u_{\min})/(u_{\max} - u_{\min})$ against the dimensionless shifted height $(y - y_{\max})/b_1$ is plotted in Fig. 8 with the fitting curve

$$\frac{u - u_{\min}}{u_{\max} - u_{\min}} = [\tanh(C_1 \cdot \xi + C_2) + 1] \cdot \{C_3 - C_4 \cdot \cos[C_5 \cdot (\xi + C_6)] \cdot e^{-\xi}\} \quad (2)$$

in which $\xi = (y - y_{\max})/b_1$, $C_1 = 1.613$, $C_2 = 1.503$, $C_3 = 0.280$, $C_4 = 14.716$, $C_5 = 0.011$, and $C_6 = 145.948$. The R^2 value of the fitting curve in the figure is 0.979. The results show surprisingly well behaved similarity corresponding to the formation of the shear layer before the passage of the solitary wave crest during $-12.0 \leqslant t\sqrt{g/h} \leqslant -6.0$ for $0 < x/h \leqslant 0.121$. Note that the data points with $u < u_{\min}$ near the tip of the vertical plate are not included in the similarity plot in Fig. 8 due to the local effect of the tiny eddy, shown in Fig. 3(c), caused by the inevitably finite thickness of the vertical plate. The scattering at $\xi > 1.0$ in Fig. 8 reflects the influence of the external velocity field induced by the approaching solitary wave. It should be pointed out that Eq. (2) at $\xi \leqslant 0$ is similar to the velocity distribution of the traditional thin shear layer flows with the momentum thickness used as the characteristic length scale (Michalke, 1965; Kuo and Chang, 1998).

3.2. Formation of a vertical jet

As stated above, the shear layer is followed by the generation and shedding of vortices and then a flow similar to a jet discharging upward along the rear edge of the vertical plate. Fig. 9 shows the vertical velocity distribution of the jet measured at several horizontal cross sections at $0.0 \leqslant y/h \leqslant 0.509$ during the period of $10.0 \leqslant t\sqrt{g/h} \leqslant 24.0$, corresponding to the period after the complete passage of the solitary wave. Each profile exhibits similar asymmetric characteristics due to the interaction between the wave and the plate. Not only is such kind of jet velocity profile different from the axisymmetric and symmetric jets (Lin et al., 1998), it is also different from the traditional wall jet

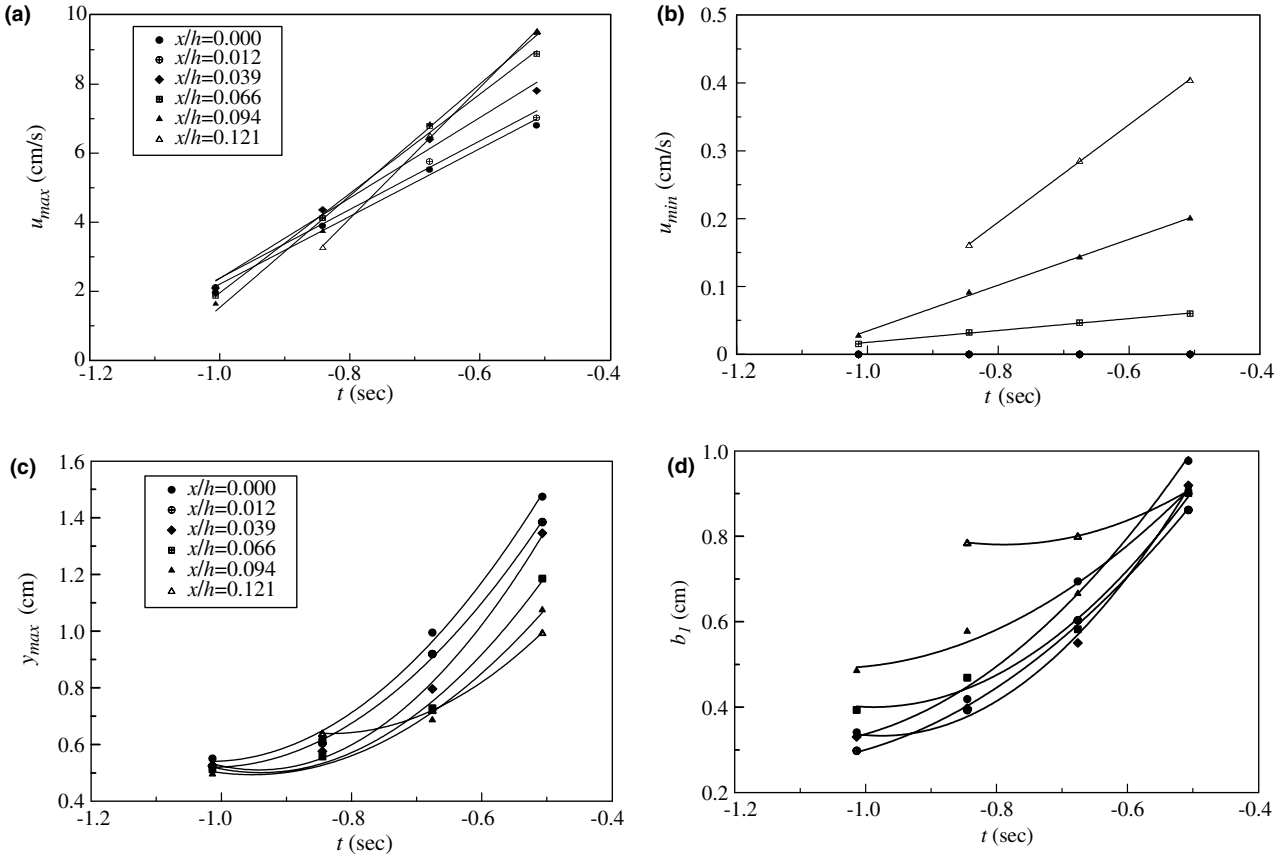

Fig. 7. Temporal and spatial variations of u_{max}, u_{min}, y_{max}, and b_1 during the period of formation of the separated shear layer.

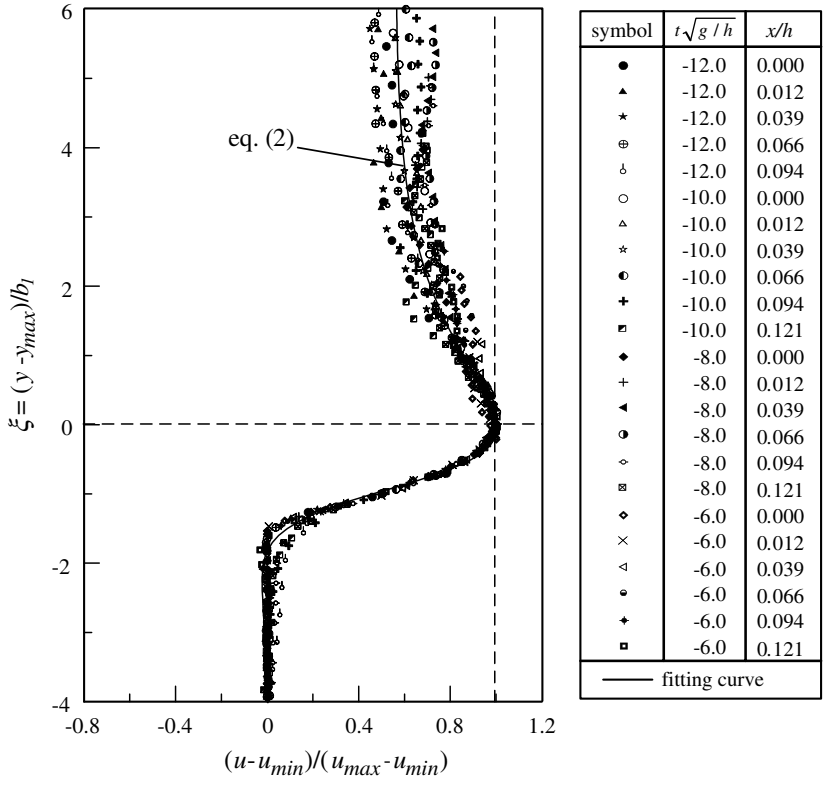

Fig. 8. Similarity profile between the dimensionless horizontal velocity deficit and the dimensionless shifted height.

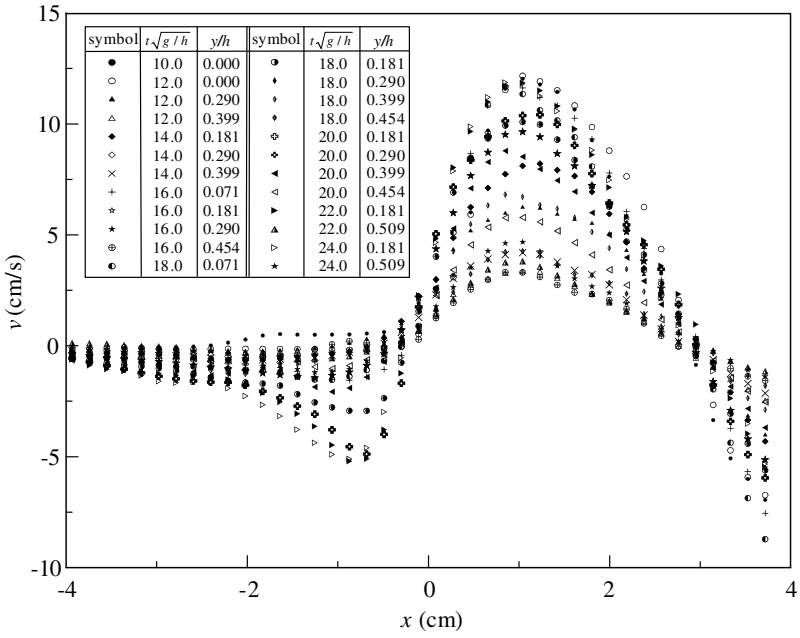

Fig. 9. Variation of the vertical velocity distributions taken at six different horizontal cross sections between $y/h = 0.0$ and 0.509.

(Rajaratnam, 1976) and the deflected wall jet of a free overfall (Lin et al., in press-b).

In order to investigate the typical profile with such an asymmetric characteristic, the concept with two different half-jet widths was developed to illustrate the variation of the vertical jet. Fig. 10 depicts the schematic velocity profile of the vertical jet. In the figure, v_{max} is the maximum vertical velocity and x_{max} is the value of x where $v = v_{max}$ occurs. b_2 and b_3 are the half-widths, defined as $|x_{1/2} - x_{max}|$ with $x_{1/2}$ defined at $v = 0.5v_{max}$ at each side of the jet axis. We expect that v_{max}, x_{max}, b_2 and b_3 may be the right velocity and length scales, and their values may vary with time and height due to the unsteady solitary wave motion. Nonlinear curve fittings to the experimental data (similar to that in Fig. 9) were also carried out to obtain more accurate estimates of these values. The variations of v_{max}, x_{max}, b_2 and b_3 with respect to time for the range of $y/h = 0.071$ to $y/h = 0.509$ are shown in Fig. 11. In Fig. 11(a), v_{max} gradually and linearly increases with respect to t for the time period of $1.0\text{ s} < t \leqslant 2.1\text{ s}$ (i.e., $10.0 < t\sqrt{g/h} \leqslant 24.0$) except that it is nearly constant at $y/h = 0.071$ (i.e., at the location slightly higher than the tip of the vertical plate), due to its location being close to the "nozzle" formed by the large vortex (see Fig. 4(f) and (g)). In Fig. 11(b), x_{max} decreases slightly with the increase of t for $y/h = 0.071$, 0.181 and 0.290, is nearly constant for $y/h = 0.399$, and increases with the increase of t for $y/h = 0.454$ and 0.509. Its value is approximately 10 mm ± 2 mm, varying within a narrow range of 2 mm. Fig. 11(c) and (d) show the temporal variations of b_2 and b_3. Similar to x_{max}, the values of b_2 and b_3 are approximately 12 mm ± 2 mm and 7 mm ± 2 mm, respectively, and both vary within a fairly narrow range. In summary, Fig. 11 shows the trends for the spatial and temporal variations of the velocity and length scales after the complete passage of the solitary wave.

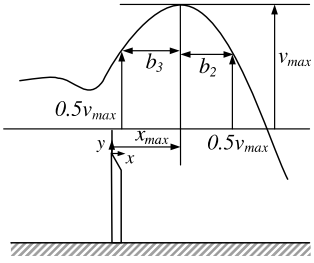

Fig. 10. Schematic sketch of the vertical jet.

In the analysis of a jet flow, it is common that the maximum velocity and the half-width of the jet are used as the characteristic velocity and length when the jet has a steady jet speed (Rajaratnam, 1976). Following the same concept and with the use of x_{max} as a reference point, the non-dimensional form of the vertical velocity v against the shifted width $(x - x_{max})$ may be obtained when normalized by the characteristic velocity scale v_{max} and the characteristic length scales b_2 and b_3 for $(x - x_{max}) > 0$ and $(x - x_{max}) < 0$, respectively. Fig. 12 shows the similarity results of (v/v_{max}) against $(x - x_{max})/b$ at $0.0 \leqslant y/h \leqslant 0.509$ during the period of $10.0 \leqslant t\sqrt{g/h} \leqslant 24.0$. Despite each of the profiles Fig. 9 exhibits asymmetric characteristics, the similarity trend is surprisingly symmetrical at $v/v_{max} > 0$. Regression analysis gives the unique similarity profile as follows:

$$\frac{v}{v_{max}} = c_1 \cdot [\exp(-0.5c_2 \cdot \varepsilon^2) - 1] + 1 \tag{3}$$

in which $\varepsilon = (x - x_{max})/b$, $c_1 = 1.878$, $c_2 = 0.623$, and $b = b_2$ for $(x - x_{max}) > 0$ and $b = b_3$ for $(x - x_{max}) < 0$. The

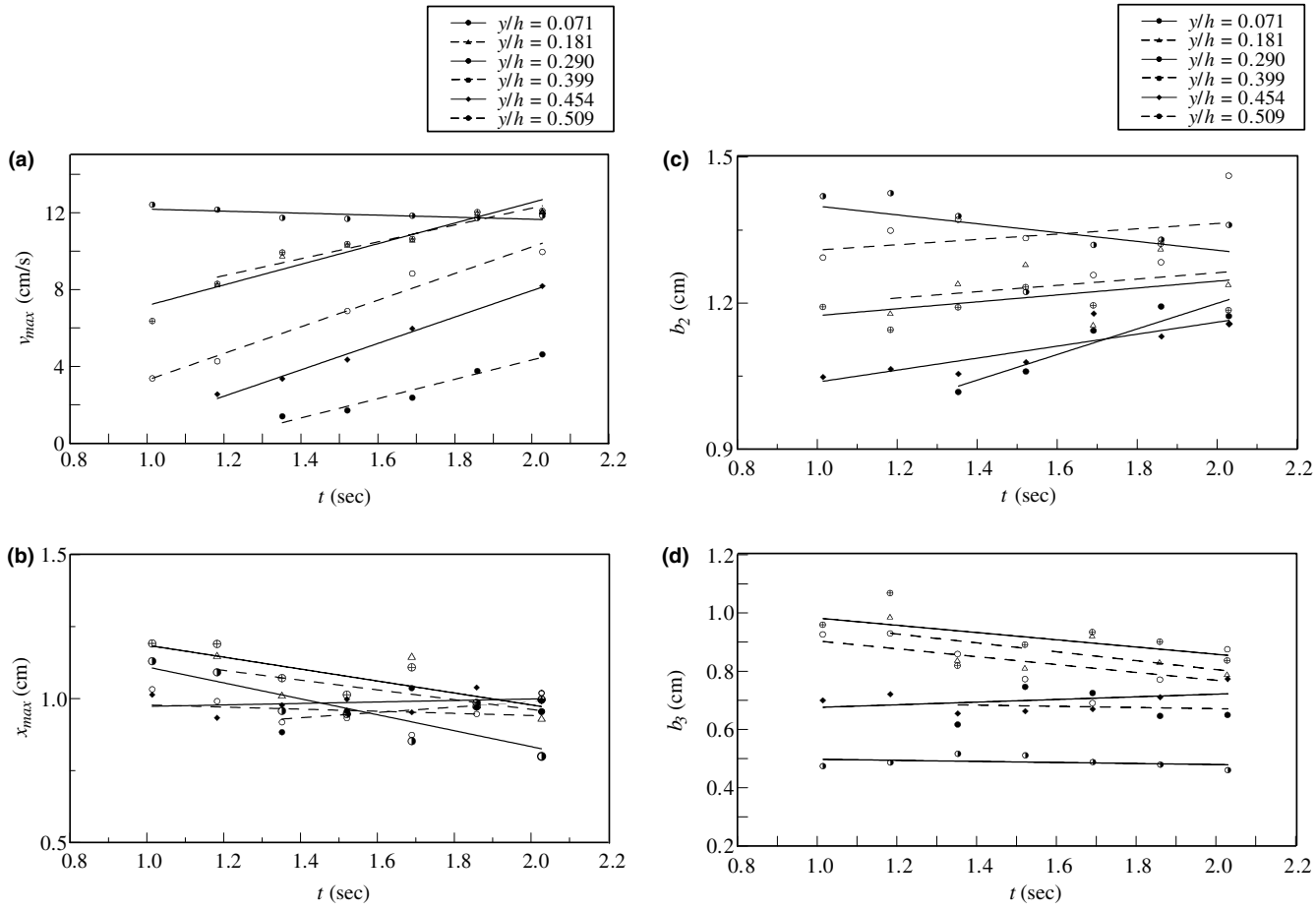

Fig. 11. Temporal and spatial variations of u_{max}, x_{max}, b_2, and b_3 during the period of formation of the vertical jet: (◑) $y/h = 0.071$; (△) $y/h = 0.181$; (⊕) $y/h = 0.290$; (○) $y/h = 0.399$; (◆) $y/h = 0.454$; (●) $y/h = 0.509$.

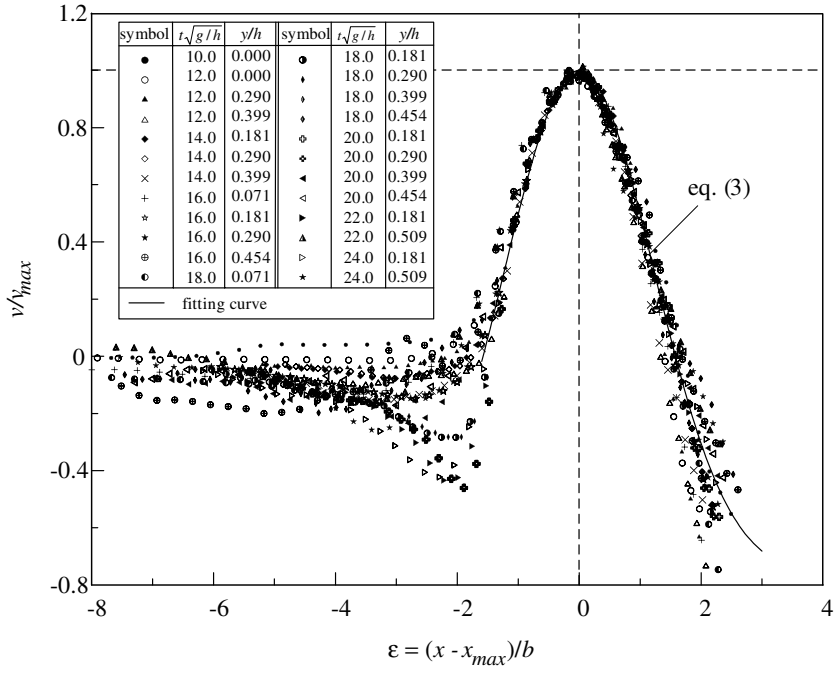

Fig. 12. Similarity profile between the dimensionless vertical velocity and the dimensionless shifted width.

R^2 value is 0.970 in the fit. Note that Eq. (3) is very similar to the velocity distribution of the traditional plane turbulent free jet (Zijnen, 1958; Rajaratnam, 1976).

It is important to point out that the evolution process of the unsteady flow field of a solitary wave passing a submerged vertical plate includes the formation of a separated shear layer, the generation and shedding of vortices, the formation of a vertical jet, and the impingement of the jet onto the free surface. Nevertheless, for the case of an approaching flow with a steady sheared stream (i.e., with upstream boundary) over a submerged vertical plate, only a steady separation bubble (or standing eddy) is formed downstream of the vertical plate, as evidenced by Good and Joubert (1968) and Gupta and Ranga-Raju (1987).

4. Concluding remarks

The detailed flow pattern and characteristics of vortex shedding induced by a solitary wave propagating over a submerged vertical plate were studied experimentally. The particle tracing technique was used for qualitative flow visualization while the particle image velocimetry (PIV) technique was used for quantitative velocity measurements. The vortex shedding process can be classified into four phases in the chronological order: (1) the formation of a separated shear layer on the rear side of the vertical plate, (2) the generation and shedding of a large vortex confined by the bottom and the vertical plate, (3) the formation of a vertical jet, and (4) the impingement of the jet onto the free surface.

Several important velocity and length scales during the time periods corresponding to the formations of the shear layer and the vertical jet were discussed. A unique similarity profile between the dimensionless horizontal velocity deficit and the dimensionless shifted height was obtained for the shear layer before the passage of the solitary wave crest. Moreover, a second unique similarity profile between the dimensionless vertical velocity and the dimensionless shifted width was also demonstrated for the vertical jet after the complete passage of the solitary wave.

Acknowledgements

The authors wish to thank the financial supports of the Directorate General of Highways, Ministry of Transportation and Communications of Taiwan, and the National Science Council of Taiwan (Grant Nos. NSC93-2625-Z-005-010 and NSC93-2611-E-005-002).

References

Chang, K.A., Hsu, T.J., Liu, P.L.F., 2001. Vortex generation and evolution in water waves propagating over a submerged rectangular obstacle. Part I: Solitary waves. Coastal Engineering 44, 13–36.

Chang, K.A., Hsu, T.J., Liu, P.L.F., 2005. Vortex generation and evolution in water waves propagating over a submerged rectangular obstacle. Part II: Cnoidal waves. Coastal Engineering 52, 257–283.

Daily, J.W., Stephan, S.C., 1953. Characteristics of the solitary wave. Transactions ASCE 118, 575–587.

Good, M.C., Joubert, P.N., 1968. The form drag of two-dimensional bluff-plates immersed in turbulent boundary layers. Journal of Fluid Mechanics 31 (3), 547–582.

Gupta, V.P., Ranga-Raju, K.G., 1987. Separated flow in lee of solid and porous fences. Journal of Hydraulic Engineering 113, 1266–1276.

Huang, C.J., Dong, C.M., 1999. Wave deformation and vortex generation in water waves propagating over a submerged dike. Coastal Engineering 37, 123–148.

Huang, C.J., Dong, C.M., 2001. On the interaction of a solitary wave and a submerged dike. Coastal Engineering 43, 265–286.

Kravchenko, A.G., Moin, P., 2000. Numerical studies of flow over a circular cylinder at $Re = 3900$. Physics of Fluids 12, 403–417.

Kuo, C.H., Chang, C.W., 1998. Shear-layer characteristics across a cavity with a horizontal top plate. Fluid Dynamics Research 22, 89–104.

Lin, P., 2004. A numerical study of solitary wave interaction with rectangular obstacles. Coastal Engineering 51, 35–51.

Lin, C., Wei, D.J., Yen, G.H., 1998. Investigation of vortex structures in the mixing layers of axisymmetric jets. Journal of the Chinese Institute of Civil and Hydraulic Engineering 10, 79–92.

Lin, C., Chang, S.C., Chang, K.A., in press-a. Laboratory observation of a solitary wave propagating over a submerged rectangular dike. Journal of Engineering Mechanics.

Lin, C., Hwung, W.Y., Hsieh, S.C., Chang, K.A., in press-b. Experimental study on mean velocity characteristics of flow over vertical drop. Journal of Hydraulic Research.

Lin, C., Hsieh, S.C., Kao, M.J., Hsu, H.Y., 2004. Study on mean velocity characteristics of near-wake flow behind a circular cylinder: application of simultaneous measurement technique by PIV and FLDV. Journal of the Chinese Institute of Civil and Hydraulic Engineering 16, 73–91.

Mei, C.C., Black, J.L., 1969. Scattering of surface waves by rectangular obstacles in waters of finite depth. Journal of Fluid Mechanics 38, 499–511.

Michalke, A., 1965. On spacially growing disturbances in an inviscid shear layer. Journal of Fluid Mechanics 23, 521–544.

Ono, M., Deguchi, I., Kubota, S., 1997. Flow pattern around bottom structure in waves. Proceedings of Civil Engineering in the Ocean 15, 895–900 (in Japanese).

Rajaratnam, N., 1976. Turbulent Jets. Elsevier Scientific Publishing Company, Amsterdam.

Sue, Y.C., Chern, M.J., Hwang, R.R., 2005. Interaction of nonlinear progressive viscous waves with a submerged obstacle. Ocean Engineering 32, 893–923.

Tang, C.J., Chang, J.H., 1998. Flow separation during solitary wave passing over submerged obstacle. Journal of Hydraulic Engineering 124, 742–749.

Ting, F.C.K., Kim, Y.K., 1994. Vortex generation in water waves propagation over a submerged obstacle. Coastal Engineering 24, 23–49.

Zhuang, F., Lee, J.J., 1996. A viscous rotational model for wave overtopping over marine structure. In: Proceedings of the 25th International Conference on Coastal Engineering, Orlando, FL, 2178–2191.

Zijnen, B.G.H., 1958. Measurements of the velocity distribution in a plane turbulent jet of air. Applied Scientific Research, Section A 7, 256–276.